AIAA JOURNAL
Vol. 32, No. 10, October 1994

Particle Dispersion in a Transitional Axisymmetric Jet: A Numerical Simulation

J. Uthuppan* and S. K. Aggarwal†
University of Illinois, Chicago, Illinois 60607
and
F. F. Grinstein‡ and K. Kailasanath§
Naval Research Laboratory, Washington, D.C. 20375

Numerical simulations are used to study the dynamics and dispersion of particles in the near field of a high velocity transitional axisymmetric jet. A time-dependent finite-difference approach that employs a fourth-order, phase-accurate flux-corrected transport algorithm is used to simulate the flow. Extensive flow visualization and analysis based on numerical simulation are employed to analyze the influence of large-scale vortical structures on the particle dynamics and dispersion. The simulations provide evidence of the existence of three distinct dispersion mechanisms, namely, the vortex, centrifugal, and inertial mechanisms, and the prominent role of vortex merging in the dispersion process. Whereas small particles get caught in the vortical structures and large particles pass through them, the intermediate size particles ride over them and tend to be flung out of the shear layer. Quantified dispersion results also show the higher dispersion of intermediate size particles (Stokes number near unity), that has been reported by previous investigators for lower velocity jets. The effects of particle density, injection location, and injection velocity on dispersion have also been studied. The predictions are also compared with previous experimental and numerical results.

Introduction

PARTICLE and droplet dispersion in turbulent shear flows is an integral part of many important technological processes. The purpose of this study is to numerically analyze the behavior of particles in the presence of large vortex structures in an axisymmetric transitional jet. Experimental and computational studies conducted in the last two decades have shown that large-scale coherent structures govern the dynamics of turbulent flows.[1] Since the flowfield is dominated by these structures, droplet dispersion is likely to be controlled mainly by them and not by small-scale turbulent fluctuations. Based on available experimental results, it was proposed[2] that the large-scale structures would impose a selective dispersion process on particles, and this process would be governed by the ratio of particle aerodynamic response time to the characteristic flow time related to the large turbulent structures. The ratio of these two time scales, also called the Stokes number *St*, was used to characterize the effectiveness of the large-scale structures to laterally disperse the particles.

Most of the previous predictive efforts involving particle dispersion in turbulent shear flows have employed flow models that use only the time average properties of turbulence. As discussed by Crowe,[2] these models do not account for the influence of large vortex structures and, thus, cannot be used as a model to understand the dynamics of dispersion. Some of the time-dependent numerical methods used the discrete vortex model approach[3–5] to simulate the flow; Chung and Troutt[5] in particular dealt with the simulation of particle dispersion in an incompressible axisymmetric jet. Lazaro and Lasheras[6–8] reported detailed experimental results on the particle dispersion in a developing turbulent free shear layer. Both naturally developing and forced shear layers were studied. Samimy and Lele[9] analyzed the slip velocity characteristics and the selective nature of droplet dispersion in a compressible free shear layer. Aggarwal et al.[10] conducted a numerical study of particle dispersion in planar shear layers using a finite-difference approach. Hishida et al.[11] used a modified laser Doppler anemometry (LDA) approach to study the behavior of spherical glass particles in a turbulent mixing layer with low gas-phase velocities. All of these studies report that higher dispersion is exhibited by intermediate size particles, characterized by the value of *St* near unity.

This work employs a finite-difference approach to simulate an axisymmetric jet evolving in both space and time. The focus of the study is to analyze the effects of large-scale structures on the dynamics and dispersion of particles in the near jet region. Extensive use of flow visualization is made to identify the mechanisms affecting the dynamics of dispersion, and the interaction of particles with the large-scale structures. The numerical algorithm used for the gas-phase calculations is based on the explicit flux-corrected transport (FCT) algorithm, which has been previously tested for jet simulations[12] and numerous other nonreacting as well as reacting flow calculations. The algorithm is first used to predict the evolution of the Kelvin-Helmholtz instability. Once the transient flow effects become negligible and a developed jet regime is attained, particles of a given size and velocity are injected from specified locations at the nozzle exit. The dynamics and dispersion of these particles as influenced by the large-scale structures are studied by solving the particle equations based on a Lagrangian approach. In the first part of the study, the trajectories of isolated particles of different diameters, injected from different radial locations, are used to analyze qualitatively the effects of location and starting time on dispersion. Then, a continuous injection of particles is simulated to analyze the dynamic interaction of particles with large-scale structures and to obtain quantitative information on particle dispersion. The trajectories and snapshots (instantaneous pictures of particles from the same location but at different times) are combined to identify the mechanisms involved in the particle vortex interactions. Quantified dispersion results show the selective dispersion process of intermediate size particles and its strong dependence on the velocity of injection, particle material density, and injection location. Finally, an attempt is made to compare our results with the previous numerical and experimental results. In

Received Jan. 28, 1994; revision received April 25, 1994; accepted for publication May 16, 1994.

*Graduate Research Assistant, Department of Mechanical Engineering. Member AIAA.

†Associate Professor, Department of Mechanical Engineering. Associate Fellow AIAA.

‡Research Physicist, Center for Reactive Flow and Dynamical Systems, Laboratory for Computational Physics. Associate Fellow AIAA.

§Head, Center for Reactive Flow and Dynamical Systems, Laboratory for Computational Physics. Associate Fellow AIAA.

this context, a recent experimental study by Longmire and Eaton[13] is found to be particularly useful.

Numerical Model

The physical system simulated is a high-speed axisymmetric free jet of air, with velocity $U_0 = 200$ m/s, emerging into quiescent ambient air. The jet, which has a diameter $D = 1.4$ cm, is assumed to be initially laminar and having standard temperature and pressure everywhere. These are idealized conditions as most experimental jets at these velocities are initially not laminar. A schematic sketch of the system is given in Fig. 1a. Here, y is the axial coordinate and x the radial coordinate. A portion of the nozzle is placed inside the computational domain. This allows the pressure at the region in and around the nozzle to respond to fluid accelerations downstream, thus enabling the instabilities to evolve naturally in the calculations.[12] Particles of diameters ranging from 1 to 50 μm ($0.02 < St < 53$) are injected from different radial locations at the nozzle exit. Since the jet is axisymmetric, a specular condition is imposed on the particles exiting the domain at the jet axis (left boundary). This assumes that for every particle exiting at the left boundary, another particle enters the domain at the reflected angle.

The numerical model for the gas phase is based on the two-dimensional, time-dependent inviscid conservation equations for mass, momentum, and energy density for an ideal gas. Particle position in the flowfield is computed by solving the equation of motion using a Lagrangian approach. The governing equations for mass, momentum, and energy density are as follows:

$$\frac{\partial \rho}{\partial t} = -\nabla \cdot (\rho \boldsymbol{V}) = S_\rho \tag{1}$$

$$\frac{\partial (\rho \boldsymbol{V})}{\partial t} = -\nabla \cdot (\rho \boldsymbol{V}\boldsymbol{V}) - \nabla p + S_v \tag{2}$$

$$\frac{\partial E}{\partial t} = -\nabla \cdot (E\boldsymbol{V}) - \nabla \cdot p\boldsymbol{V} + S_e \tag{3}$$

$$E = e + (1/2)\,\rho\,(V_y^2 + V_x^2) \tag{4}$$

$$e = p/(\gamma - 1) \tag{5}$$

In the preceding equations ρ, p, e, $\boldsymbol{V}$, and γ are the density, pressure, internal energy, velocity vector, and specific heat ratio, respectively. The terms S_ρ, S_v, and S_e denote the source terms due to the exchange of mass, momentum, and energy with the dispersed phase, respectively. In the present study, these terms can be ignored since the objective is to study the effect of large-scale structures on the particles' dynamics and dispersion. The particles' influence on the gas phase would be negligible since an ultradilute two-phase flow is being simulated.

A Lagrangian approach is followed to predict the particle motion in the jet flow. The trajectory of each particle is computed using the equations of motion, and it is assumed that the drag force is the only dominant force acting on it. The dynamic equations for the velocity and position of each particle can be written as

$$\frac{d\boldsymbol{X}_p}{dt} = \boldsymbol{V}_p \tag{6}$$

$$\frac{d\boldsymbol{V}_p}{dt} = \frac{F}{(4/3)\,\pi r_p^3 \rho_p} \tag{7}$$

where X_p, V_p, ρ_p and r_p are the position and velocity vector, density, and radius represented by the subscript p for a particle, respectively. All particles are considered to be nonevaporating spheres and the particle density ρ_p is assumed large compared to the fluid density ρ. In this paper, the term particle is used rather than the term droplet to signify that particles are rigid spheres. Water particles in a jet of air, considered in our study, give an approximate ρ_p/ρ ratio of 10^3. This sufficiently large value allows us to neglect the Basset force,[6] pressure gradients, and other contributions from flow nonuniformities and consider only the drag force as the force term F in Eq. (7). Moreover, using a scale analysis, Lazaro and Lasheras[6] have identified the conditions when the additional forces can be neglected. These conditions are also applicable to our study. Other forces including gravity and particle-particle interaction are also neglected in this analysis. The ratio of gravity force to drag force for a Stokesian flow is given as $(\rho_p d_p^2 g)/(18\mu V_d)$, which for a 50-μm water droplet in a 200.0-m/s air jet is approximately 10^{-3}. For a non-Stokesian flow, the ratio will be even smaller. Also, the range of particle sizes where the dispersion is significant is below 30 μm, and the given ratio will be reduced further. The particle-particle interaction is negligible since an ultradilute two-phase flow is being simulated. The drag force is given by

$$F = C_d\,(1/2)\,\pi r_p^2 \rho |\boldsymbol{V} - \boldsymbol{V}_p|\,(\boldsymbol{V} - \boldsymbol{V}_p) \tag{8}$$

where the drag coefficient C_d is given by the solid sphere drag correlation as

$$C_d = \frac{24}{Re_p}\left(1 + \frac{Re_p^{2/3}}{6}\right) \tag{9}$$

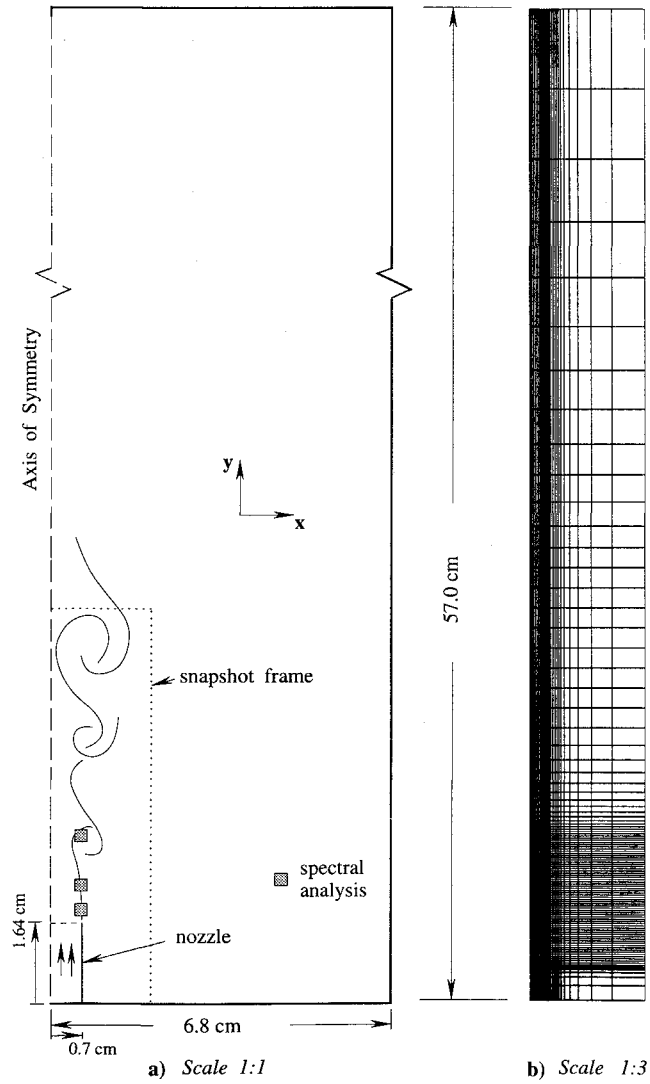

Fig. 1 Computational domain.

Table 1 Stokes numbers for various particle diameters, $\rho_p = 1$ g/cm^3

d_p, μm	St	d_p, μm	St
1	0.02	10	2.12
2	0.08	12	3.06
5	0.53	14	4.17
6	0.76	20	8.50
7	1.04	30	19.13
8	1.36	50	53.15

and

$$Re_p = \frac{2\rho|\boldsymbol{V}-\boldsymbol{V}_p|r_p}{\mu} \tag{10}$$

The computational domain is 57.2 cm long in the streamwise (Y) direction and 6.8 cm in the radial (X) direction. Note that the grid given in Fig. 1b is of a smaller scale with only every fifth grid line shown. For the computations done in this study, the grid is nonuniform with 122 nodes in the radial direction and 422 nodes in the streamwise direction. The cells are closely spaced, minimum spacing being 0.01 cm, in the shear-layer region immediately following the nozzle exit and become farther apart as the distance from the nozzle edge increases both in the radial and axial directions. The minimum spacing of 0.01 cm in the simulated shear-layer region also gives an effective initial momentum thickness θ_0. This initial thickness gives a reference length scale for describing the jet flow in the initial region. The near jet region considered in this work is mainly characterized by θ_0, and to a lesser extent also by the jet diameter D. Farther downstream, the jet diameter becomes the effective length scale, and the dominant instability mode is the preferred jet mode; see Refs. 14 and 15. The observed jet shear-layer instability frequency, $S_{\theta 0} = f_{\theta 0}/U_0 \approx 0.014$, is found to be in the expected range 0.0125–0.0155 of the laboratory experiments.[16] In the present study, the largest characteristic flow time affecting the dispersion is that associated with the second vortex-ring pairing, $t_f = 1/(f/4)$. This time is chosen to compute the Stokes number St, given by the relation

$$St = t_p/t_f \tag{11}$$

where the particle response time t_p is

$$t_p = \frac{\rho_p d_p^2}{18\mu} \tag{12}$$

Here, d_p is the particle diameter and μ the fluid viscosity. The particle time t_p is a measure of the aerodynamic responsiveness of the particle. The Stokes numbers for selected particle sizes used in our calculations are given in Table 1.

Inflow and outflow boundary conditions developed and tested for multidimensional FCT calculations are used to represent the effects of the region outside the computational domain. Grinstein et al.[12] gives a detailed description of the boundary conditions used in the gas-phase calculations. The initial location and velocity, X_{inj} and V_{inj}, respectively, of the particle must be specified for integrating the particle equations. The initial axial location for all of the particles is the nozzle exit, which is $Y = 1.63$ cm. The radial location and velocity are varied for different cases.

The simulation employs the monotone integrated large eddy simulation (MILES) algorithm[17] to solve the Eulerian gas-phase equations. The particle equations are integrated using a second-order Runge-Kutta procedure. The gas-phase algorithm is based on a fourth-order phase-accurate, FCT, time-splitting procedure. For numerical stability, the chosen time step Δt was 10^{-7} s, which enables the Courant number to be less than one (0.4–0.5) with the selected grid spacing. The Courant number here is based on the smallest grid spacing and the velocity equal to the speed of sound plus the jet initial velocity. Starting at time $t = 0$, the gas-phase equations are integrated to simulate the dynamics of the large-scale vortical structures. After some time is elapsed, when the initial transient effects become negligible, particle injection is started. Note that once the particles are in the domain, they can be anywhere within a cell and not necessarily in the center. A two-dimensional second-order interpolation is employed to calculate the gas-phase properties like density and velocity at the instantaneous particle positions.

Results and Discussion

Numerical Validation

The gas-phase algorithm (MILES) used in the present simulation has been well tested previously and shown[12,17,18] to reproduce the large-scale features of a variety of flows that are observed in the laboratory experiments. These include the Strouhal number for the shear-layer rollup and vortex mergings, the spatial distribution of vortex mergings, and the shear-layer growth rate. We performed a further independent validation and computed the jet shear layer instability Strouhal number = 0.014, which is in the expected range of 0.0125–0.155 of the laboratory experiments.[16] In addition, the Strouhal number based on the jet diameter and the second vortex-pairing frequency is 0.49, which is also in the reported range of experimental results. For the particle calculations, the effect of temporal step size on the predicted particle trajectory is shown in Fig. 2. The trajectories of 2- and 50-μm particles, injected from two radial locations, $X_{\text{inj}} = 0.5$ and 0.68 cm, are compared for $\Delta t = 10^{-7}$ and 2×10^{-7} s. As evident from the figure, the particle calculations are virtually independent of the temporal step size, validating our choice of $\Delta t = 10^{-7}$ s for all of the calculations and the use of the second-order Runge-Kutta method. Also note that $\Delta t = 10^{-7}$ s corresponds to a time that is about 1/30 of the response time of the smallest particle (1 μm) in the present study.

Particle Trajectories: Effect of Injection Location and Starting Time on Trajectories

Trajectories are plotted by tracking the instantaneous positions of a single particle as it moves through the flow region. Trajectory plots basically serve two purposes. First, they provide a qualitative picture of the dispersion process and, when done for several injection times, show the overall trend in the dispersion of different size particles. Second, they can be used to identify and analyze the different mechanisms, discussed later, responsible for particle dispersion and the role of large vortical structures in the dispersion process.

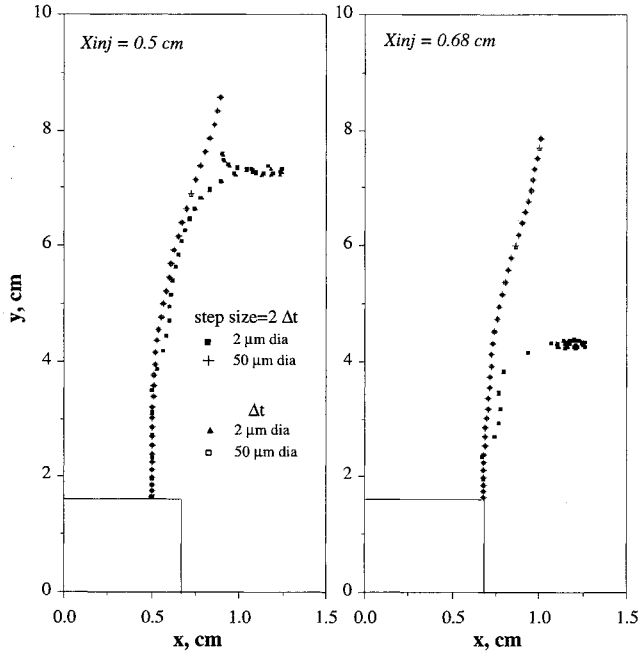

Fig. 2 Comparison of trajectories for particle calculations done every Δt and $2\Delta t$, $\Delta t = 10^{-7}$ s; period 1.5–2.2 ms or 20 shear-layer rollups.

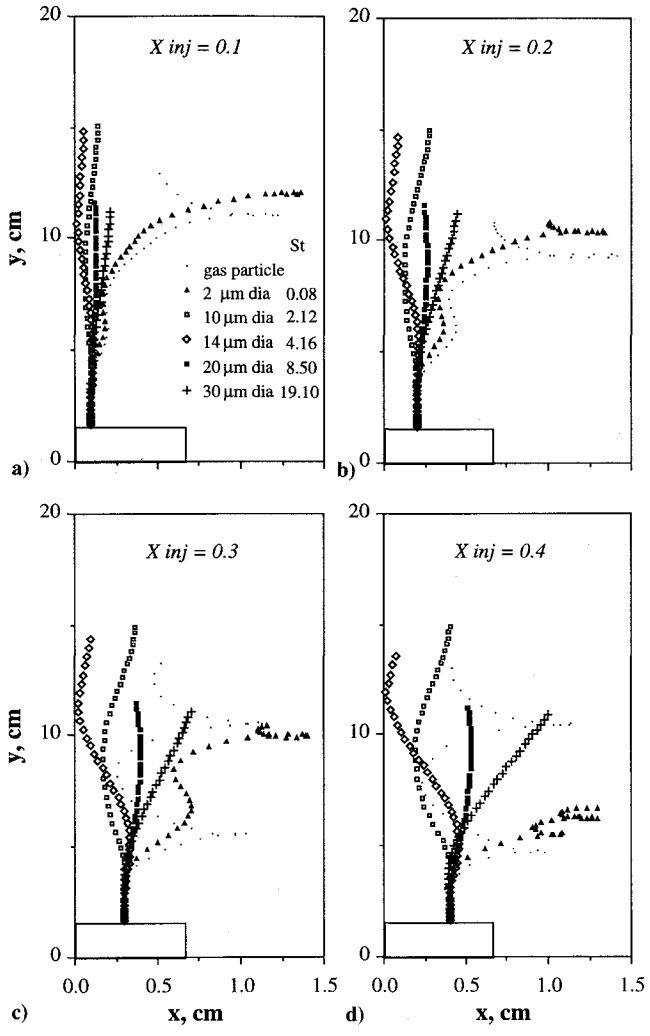

Fig. 3 Trajectories of particles injected from different locations; period 2.0–2.8 ms or 22 shear-layer rollups.

For the trajectory results presented, particle sizes ranging from 1–50 μm diameter with an injection velocity of 50 m/s (one-fourth of the jet velocity) are used. This provides a Stokes number range of 0–50. Since particles can emerge from any radial location, injection was simulated from eight different locations at the nozzle exit. Results shown for locations such as X_{inj} = 0.4 cm or less reflect particles released from the core region and those around X_{inj} = 0.68 cm represent the shear-layer region.

Figures 3 and 4 show trajectories of particles injected from eight different locations. In these figures, particle refers to the tracer (gas) particle, and the "2 μm dia" (Stokes number = 0.08) refers to the particle of diameter = 2 μm. The important observation from Fig. 3 is that for injection well inside the core region (X_{inj} < 0.3 cm), only small particles ($d_p \approx 2$ μm) are strongly influenced by the vortex ring structures. The trajectories of intermediate size (d_p 10 ≈ μm) and large ($d_p \approx 30$ μm) particles are only slightly influenced. Even the small particles are not strongly influenced by the flow structures until they move beyond the axial location y = 8.0 cm ($y/D \approx 6$), where they are entrapped in the structures. Note that this region corresponds to the third vortex pairing location, as indicated by the detailed flow visualization and spectral analysis. Beyond this location, the jet flow is expected to be dominated by the three-dimensional structures. For this reason, the results of present simulations, especially the quantitative results on particle dispersion, are confined to axial locations $y/D < 6$. Figures 3c and 3d indicate that for injection locations $X_{inj} \geq 0.3$ cm, the small particles are entrapped in the vortex rings at the second merging location (y ≈ 4.2 cm). Generally speaking, as the injection location moves closer to the shear layer, the small particles begin to get entrapped in the vortical structures sooner than before and the overall trajectory pattern begins to change. Particles flung out of the shear layer on the right tend to slow down and remain in that deflected path (Figs. 4b–4d). They do not get back into the stream as there is only negligible amount of fluid motion in this stagnant region. It is also interesting to note that for $X_{inj} > 0.4$ cm, the 2-μm particle seems to have been entrapped in the vortical structures and then flung out of it, with the implication that for these injection locations, even particles as small as 2 μm diameter can exhibit greater dispersion than the fluid particles. This result is confirmed by the quantitative data on particle dispersion presented later. The prominent role of the second pairing ($y \approx 4.2$ cm) in dispersing the particles far and wide is clearly evident at these locations. Not only the small particles, but also the intermediate size ($d_p \approx 10$ μm) and large ($d_p \approx 30$ μm) particles, injected from $X_{inj} > 0.6$ cm, are significantly dispersed by the second vortex merging.

Snapshots of Particles

Snapshots of particles give the instantaneous picture of the flowfield at any given time and clearly show the influence of merging locations on particle dispersion. The gas particles, since they follow the flowfield, give a clear picture of the large vortical structures in the developing flowfield. Because of their two-dimensional nature, the simulations only capture the large-scale features of the flow in the near jet region. Farther downstream, the three-dimensional (azimuthal) effects, not considered in the present calculations, become increasingly more important, and the two-dimensional vortex ring picture becomes physically less real-

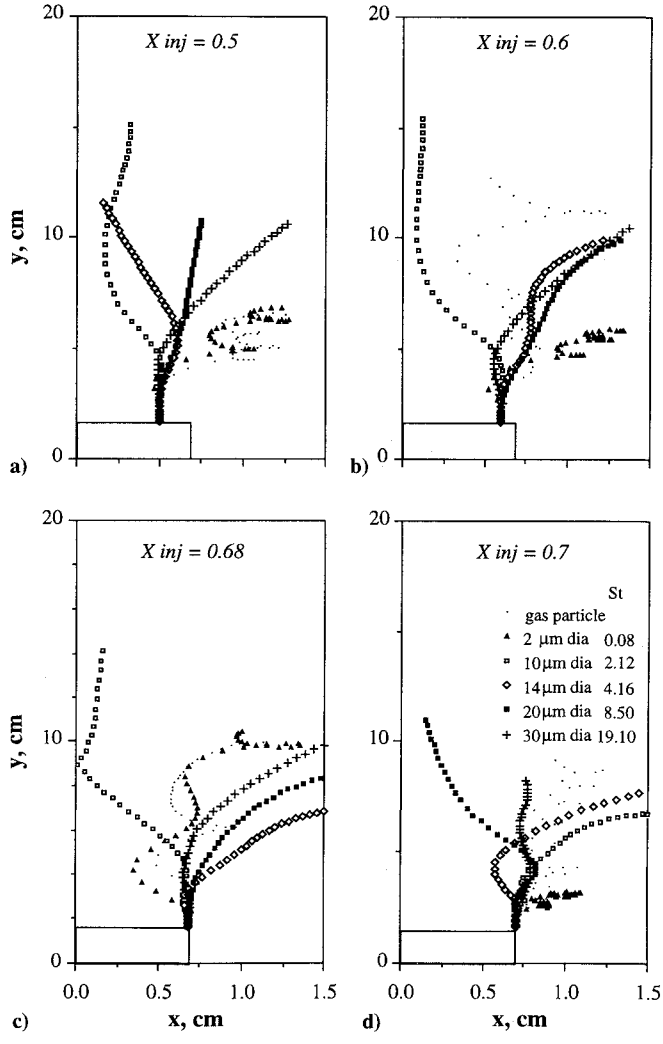

Fig. 4 Trajectories of particles injected from different locations; period 2.0–2.8 ms; D, nozzle diameter: a) $2X_{inj}/D$ = 0.71, b) $2X_{inj}/D$ = 0.86, c) $2X_{inj}/D$ = 0.97, and d) $2X_{inj}/D$ = 1.0.

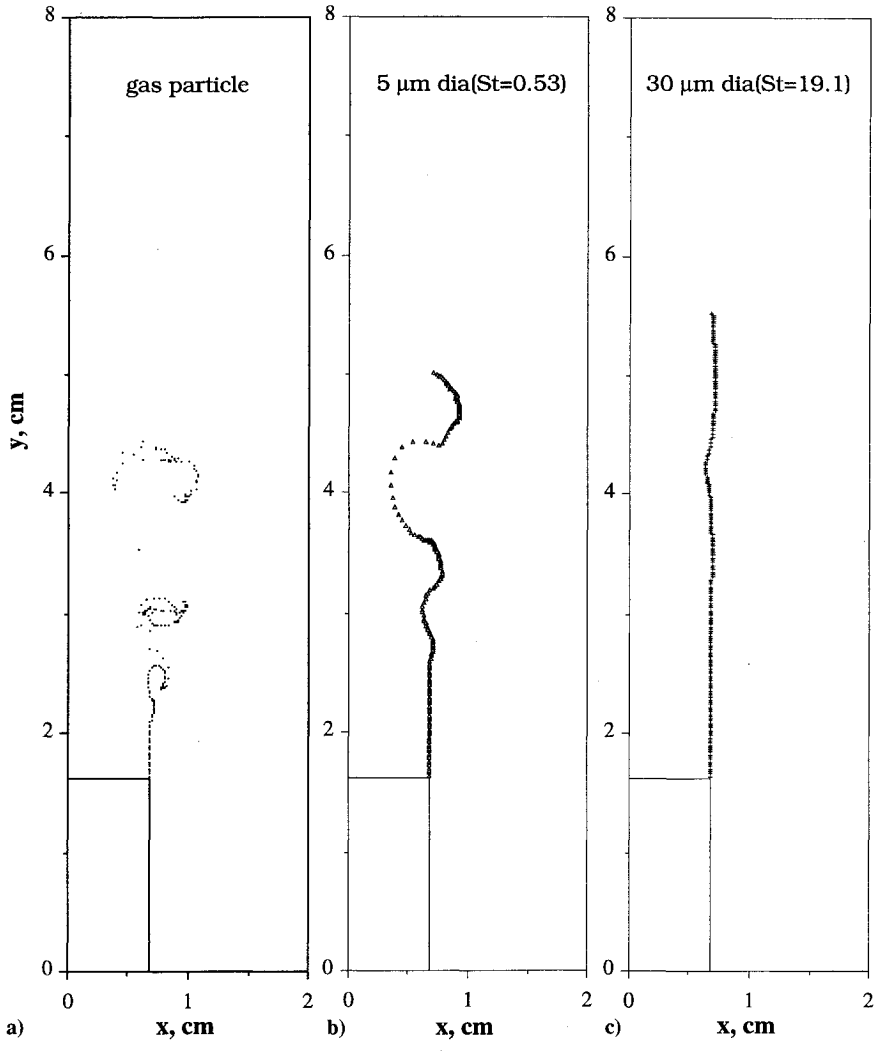

Fig. 5 Snapshots at 1.7 ms of continuously injected particles; start time = 1.5 ms and injection velocity = 200.0 m/s.

istic as a model of an axisymmetric jet.[19] For this reason, the snapshots and dispersion calculations are all done within the near jet region ($0 \le y \le 8$ cm or $0 \le y/D \le 5.7$).

Figures 5 and 6 show the snapshots of the frame at 1.7 and 2.0 ms, respectively, for gas particles, and 5- and 30-μm-diam particles. The injection is started at 1.5 ms and continued every 10 Δt. In these frames we see the gradual distribution of the particles as they move into the flowfield. Notice the wider spreading of the 5-μm particles as compared to the gas particles or the larger 30-μm particles. Also seen in Fig. 6b are the 5-μm particles gathered around the periphery of the vortical structures at $y \approx 4.1$ cm ($y/D \approx 3$). It is clear from this picture that the second pairing at this location is most responsible for the higher lateral dispersion of intermediate size particles. The 30 μm with its large momentum is hardly affected by vortical structures until it encounters the really large structures at the end of potential core. At time 2.0 ms, a total of 500 particles of each size is present in the computational domain, not all of which appear in these frames.

Particle Motion Through Vortex: Dispersion Mechanisms

Both the trajectory plots in Figs. 3 and 4 and the snapshots of particles in Figs. 5 and 6 provide a good qualitative picture of the influence of vortex ring structures on particle dynamics in the near jet region. The overall picture emerging so far is that the particles injected inside the jet core ($X_{inj} < 0.4$ cm) are not significantly influenced by the ring structures. However, as the injection location moves closer to the shear layer, there is a progressively stronger effect of the structures on particle convection. Whereas the trajectories of large particles are modified somewhat, the motion of intermediate size particles is strongly influenced; they get trapped on the periphery of the ring structures and are then flung out of them. The small particles on the other hand are able to ride with the structures.

To gain further insight into the influence of ring structures, an attempt is made to characterize the mechanisms involved in the particle dispersion process. A single particle of each size is injected at the gas velocity from a fixed location, and its instantaneous position is shown in several frames, where each frame is a snapshot at that instant in time. The gas particles continuously injected prior to the particle injection give a clear picture of the vortical structure at each instant. Both the particle motion and the snapshot of gas particles are shown in a frame of stationary vortical structures, which are convecting at approximately one-half the jet velocity.

From such studies, the particle dispersion appears to be mainly the result of three basic mechanisms, namely, the vortex, centrifugal, and inertial mechanisms. The vortex mechanism is responsible for the dispersion of particles with very low inertia, whereby the particles are able to ride with the vortex structures and exhibit dispersion behavior similar to that of tracer particles. The centrifugal mechanism is in play when particles are flung out of the spinning vortical structures by their centrifugal force. The inertial mechanism is responsible when particles are not entrapped in the vortical structures, but their trajectories and dispersion behavior are still influenced by the induced flow around them. All three mechanisms are captured in the simulations presented here.

First, let us analyze the centrifugal mechanism featured in Fig. 7. The particles are injected at time 2.0 ms from $X_{inj} = 0.68$ cm. For

convenience, only 2, 5, and 50-μm particles are shown in the initial frames where they travel in a cluster. Close scrutiny of time frames 2.05, 2.08, and 2.10 ms reveals that the 2- and 5-μm particles go around the left of 50 μm at the first pairing location ($y \approx 3.1$ cm, $y/D \approx 2.2$). At the second pairing location ($y \approx 4.2$ cm, $y/D \approx 3.0$), the particles get a sudden thrust from the spinning vortical structures there and get flung out in all directions. Frame 2.3 ms shows the particles clearly spread out in the order of their increasing inertia. The time when a given particle gets flung out depends on its size; the larger the size, the later it is thrown out. We also see the 1-μm particle getting caught inside the vortex and behaving like a tracer particle, i.e., the vortex mechanism, and the 50-μm particle follows an almost straight trajectory, although its motion is somewhat influenced by the induced flow, which we term the inertial mechanism. Figure 8a gives the apparent trajectories of particles as seen in a stationary frame of vortical structures. This gives the relative motion of the particles with the vortical structures, and again we see all three mechanisms at work.

To see the effect of these mechanisms further, let us analyze the trajectories of particles injected from $X_{inj} = 0.5$ cm starting at the same time 2.0 ms. Figure 8b shows how the influence of the three mechanisms on different size particles changes with the injection location. The particle sizes that are subjected to the centrifugal mechanism are in the range 2–6 μm, and the larger sizes (> 7 μm) are subjected to the inertial mechanism. The last symbol in all of the trajectories is the particle position at 2.3 ms.

Quantitative Dispersion Analysis

The dispersion function for each particle size is computed to quantify the dispersion behavior and to substantiate the qualitative arguments presented so far. The dispersion function is given by the relation

$$D(t, N) = \left[\left\{ \sum_{i=1}^{N} (X_i(t) - X_{io})^2 \right\} \Big/ N \right]^{1/2} \tag{13}$$

where N is the total number of particles in the flowfield at time t, X_i the radial location of particle i at time t, and X_{io} the radial injection location of the same particle at nozzle exit. An injection interval of $10\Delta t$ (0.001 ms) was used for all of the particles which were injected at the gas velocity of 200 m/s for the base case. The axial and radial domains, see Fig. 1, used in the dispersion calculation are 8.0 cm (5.7 jet diameters) and 2.0 cm, respectively. Dispersion vs size plots are done to analyze the effects of injection location, particle material density, and injection velocity.

In the chosen near jet region, the dispersion increases with time initially and levels out after about 0.8 ms (Fig. 9a). This was concluded after simulating continuous injection for a total time of 1.5 ms (duration for 42 rollups in the shear layer). For the dispersion vs size plot, shown in Fig. 9b, an average of the dispersion function values after this initial lapse of 0.8 ms, is taken for each particle size. Figure 9 provides a quantitative confirmation of the observations, made earlier, regarding the role of vortex ring structures on particle dispersion in the near jet region. The enhanced dispersion of particles in the size range 2–14 μm is due to the centrifugal mechanisms. The larger size particles are dispersed due to the induced flow around them, termed here the inertial mechanism, and the amount of dispersion is a function of their inertia.

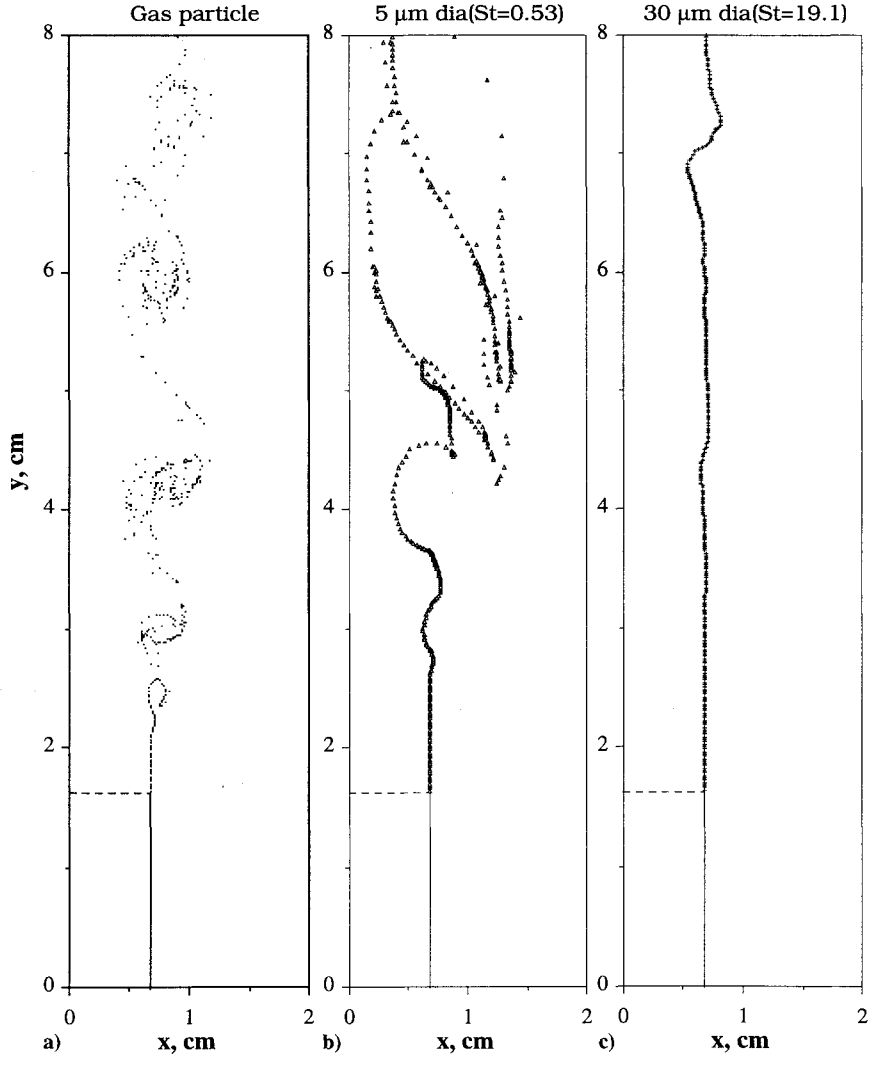

Fig. 6 Snapshots at 2.0 ms of continuously injected particles; start time = 1.5 ms and injection velocity = 200.0 m/s.

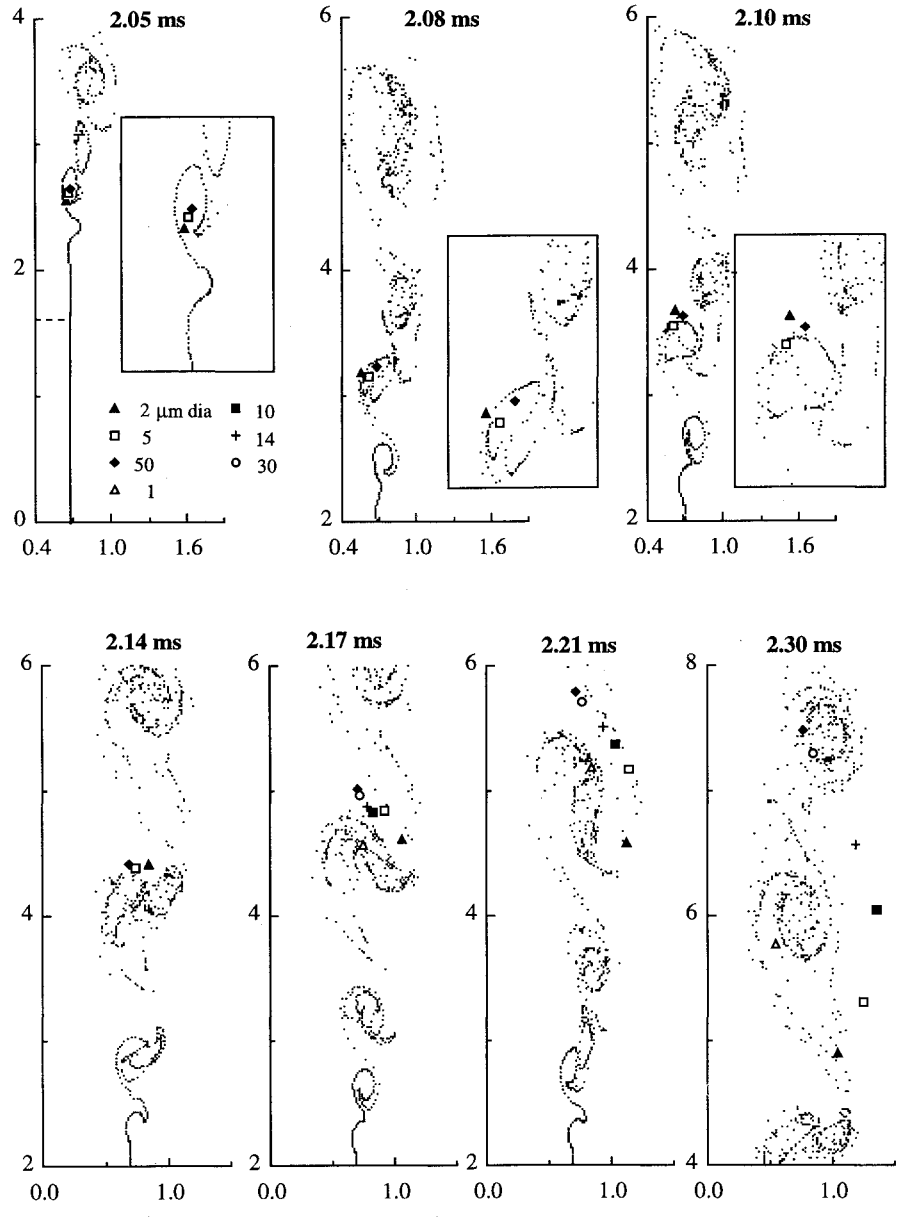

Fig. 7 Snapshots of particles injected at 2.0 ms in the vorticity field, X_{inj} = 0.68 cm, V_{inj} = 200 m/s, period 2.0–2.3 ms.

To assure that the dispersion statistics are independent of the number of particles used and the starting injection time, two results are shown in Fig. 10. As indicated in Fig. 10a, the dispersion function plot remains essentially the same when the particle injection frequency is changed. The effect of starting injection time on the predicted dispersion behavior is portrayed in Fig. 10b. Again the dispersion statistics are seen to be independent of the starting time.

Figure 11a shows the effect of injection velocity on particle dispersion. Three cases V_{inj} = 200, 100, and 50 m/s are compared. The jet velocity is 200 m/s. All are for the same injection location at X_{inj} = 0.68 cm for time period 1.5–2.7 ms or 34 shear-layer rollups. An important observation is that the particle dispersion can be significantly enhanced by reducing the injection velocity compared to the jet velocity. Not only does the maximum dispersion increase, but also the range of particle sizes for enhanced dispersion widens as the injection velocity is lowered. In addition, the maximum dispersion occurs for a larger particle size. Figure 11b gives the nondimensional dispersion vs Stokes number for the same cases. Nondimensional dispersion is defined as the ratio of particle dispersion to the gas particle dispersion. For the base case V_{inj} = 200 m/s, the enhanced dispersion is shown by particles with Stokes numbers between 0.1 and 4. By decreasing the particle injection velocity, the Stokes number range for enhanced dispersion can be significantly increased, with the important implication that the centrifugal mechanism is operative over a wider range of Stokes number.

Figure 12 shows the effect of particle density on dispersion. Five different densities ρ_p are compared: 0.2, 0.5, 1.0, 2.5, and 3.5 g/cm^3 of which 1.0 g/cm^3 is the base case. The important observation is that as the density decreases, the optimum particle size, for which the dispersion is maximized, increases. This can be explained by using Eqs. (11) and (12). If one assumes that the maximum dispersion occurs at a fixed Stokes number, and since the characteristic flow time is unchanged, this implies an increase in the optimum particle size as the density decreases. It is also interesting to note that the maximum value of dispersion is essentially independent of the density. Figure 13 compares the particle dispersion for three different injection locations at the nozzle exit X_{inj} = 0.3, 0.5, and 0.68 cm. The X_{inj} = 0.3, being very much within the core, shows the least amount of overall dispersion. Around size 4 μm, notice the sharp decline in this curve compared to a more gradual decline for X_{inj} = 0.5 cm which is closer to the mixing layer. The particle size for the maximum dispersion reduces to 2 μm for X_{inj} = 0.3 cm, as from this location only particles with very low inertia can be pulled into the mixing layer. These results substantiate

the observations made earlier as to how the three dispersion mechanisms become operative as the injection location is changed.

Comparison with Previous Experimental and Numerical Results

Finally, an attempt is made to compare our numerical results with the previously reported experimental and numerical studies. Surprisingly, we could not find much data in the literature focusing on particle dispersion in the near jet region, even though the particle-laden jets have been studied extensively. There is a numerical study, due to Chung and Troutt,[5] which reports the reciprocal of the Schmidt number *Sc* as a function of the Stokes number. Note the reciprocal of the Schmidt number represents the particle dispersion function, normalized by the dispersion function of gas particles. Figure 14a compares our results with those of Chung and Troutt and two experimental studies.[20,21] Note that in the experimental studies, the measurements were made in the far jet region, and, therefore, fail to capture the enhanced dispersion for the intermediate size particles. Although it is difficult to make a true comparison in these circumstances, our results compare favorably with the previous numerical and experimental data. Another experimental study, reported by Goldschmidt et al.,[22] indicates enhanced particle dispersion at a much lower Stokes number. This may be because the particles are not injected into the shear layer. To include their result, the dispersion data is shown on a log plot scale in Fig. 14b. Again, the overall comparison appears favorable.

A recent experimental study by Longmire and Eaton[13] is particularly relevant to the present work. They employ detailed flow visualization to examine the behavior of solid particles in the near jet region dominated by vortex ring structures and conclude that the

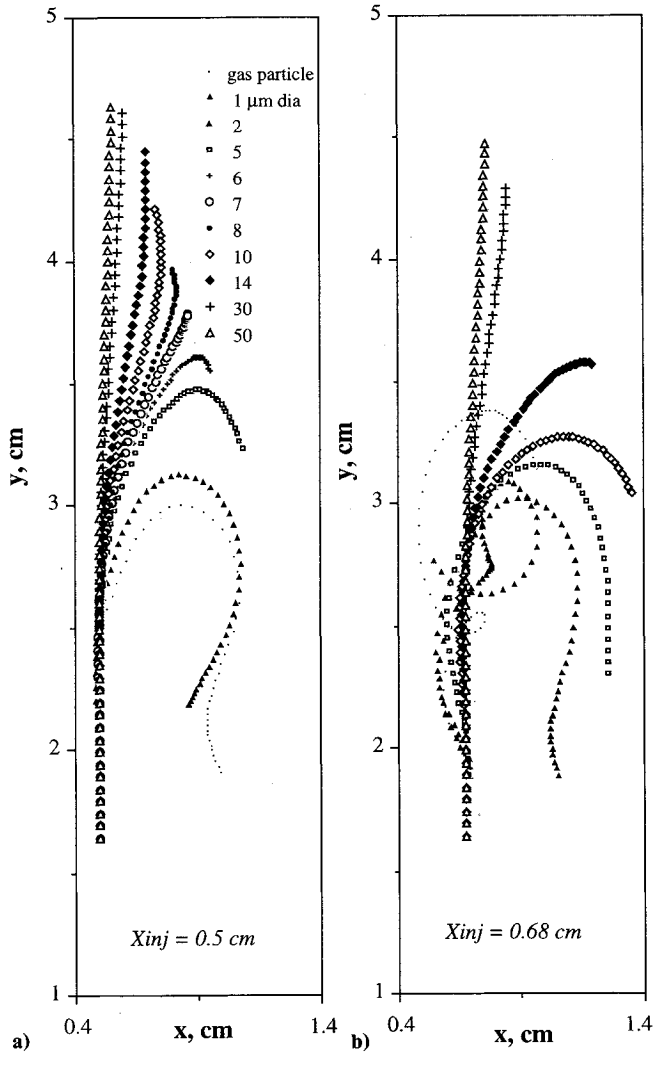

Fig. 8 Apparent trajectories of particles injected at 2.0 ms in a frame of stationary vortical structures; injection at $2X_{inj}/D = 0.71$ and 0.97.

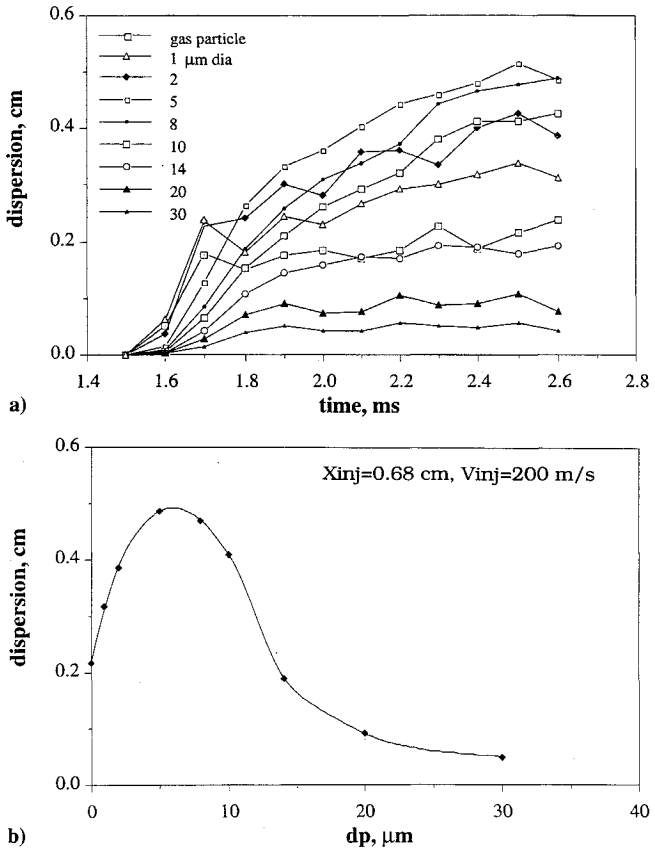

Fig. 9 Dispersion function: a) plotted as a function of time for different particle diameters and b) plotted as a function of particle diameter.

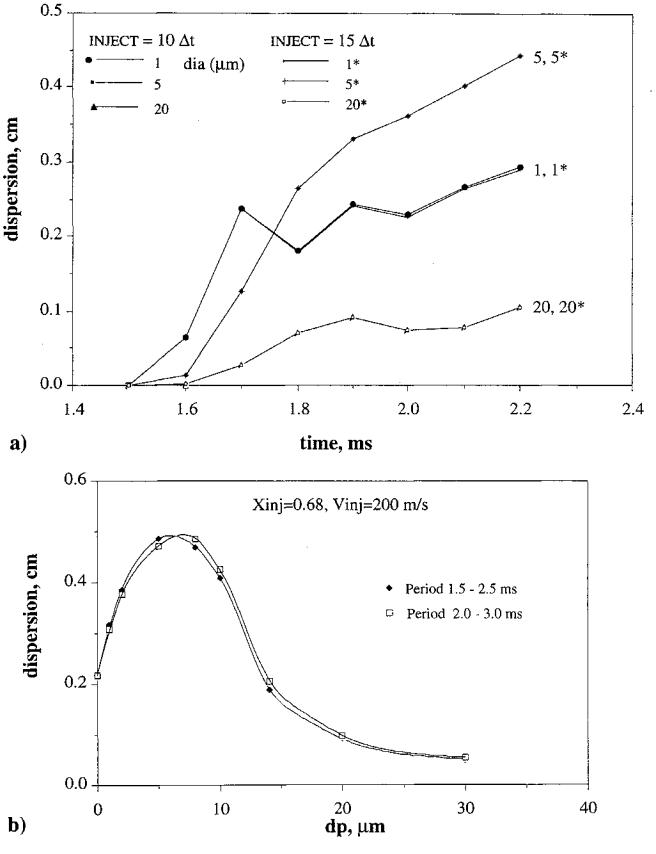

Fig. 10 Particle dispersion vs time: a) effect of injection interval on dispersion behavior; INJECT= $10\Delta t$ and $15\Delta t$ indicates injection of particles every $10\Delta t$ and $15\Delta t$, respectively, $\Delta t = 10^{-7}$ s and b) effect of starting injection time on dispersion behavior.

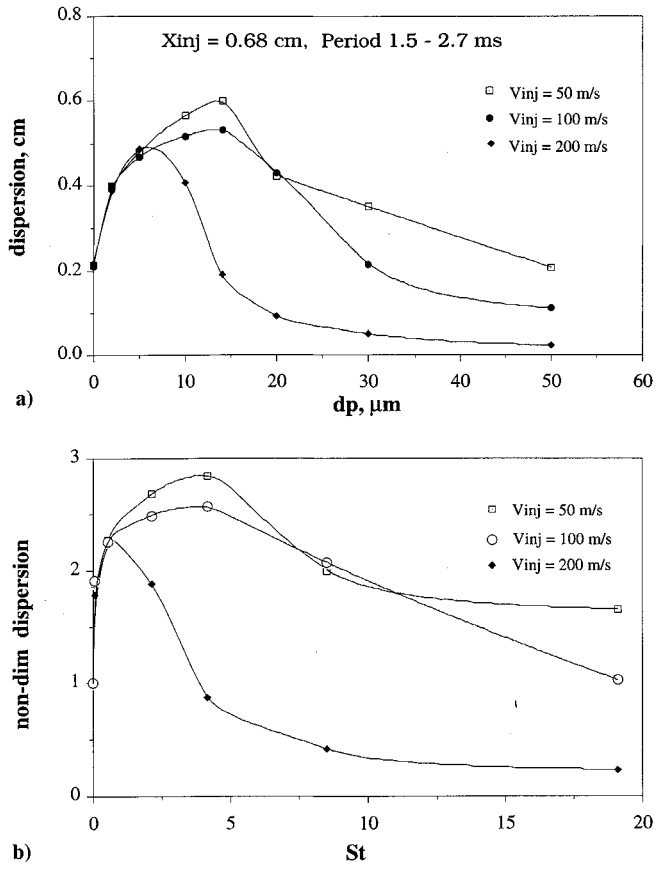

Fig. 11 Effect of injection velocity on dispersion: a) dispersion function vs particle diameter and b) nondimensional dispersion function vs Stokes number, X_{inj} = 0.68 cm, and time period for dispersion calculation 0.15–0.27 ms or 34 shear-layer rollups.

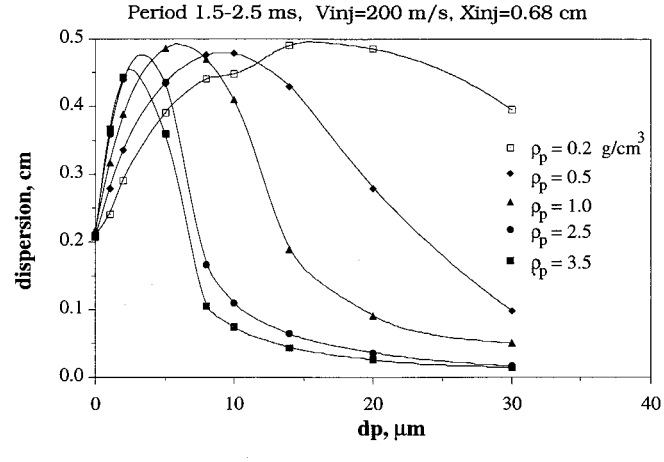

Fig. 12 Effect of particle density on dispersion, gas density 1.17 × 10^{-3} gm/cm^3; X_{inj} = 0.68 cm.

particle dispersion is governed by convection due to large-scale vortex structures. Although they do not report quantitative data on particle dispersion that can be used for direct comparison, their study corroborates our numerical result in several important aspects. First, the experimental study finds that the particles tend to wrap around the outer edges of the large vortices, which is what we have observed in our snapshots of intermediate-size particles (see Fig. 6). The experiments also reveal that particles form a cluster in the core region before being forced out by the vortex rings. We observe a similar pattern for the particles released in the outer part of the core region. Third, the experimental study observes enhanced particle dispersion in the range of Stokes number 7–12. However, note that the lowest Stokes number in the experiments is 7, limited by the smallest particle size, and the particles are injected at about one-half the jet velocity. For the same conditions ($V_{inj} = 0.5V_j$) in our study, the enhanced dispersion is observed for the Stokes numbers range 0.1–19 for particles injected in the shear layer, and as the injection location moves in the core region, the upper limit decreases. In addition, our results indicate that by decreasing the particle injection velocity, the range or the upper limit of Stokes number for enhanced dispersion can be increased. For example, by reducing the injection velocity from $V_{inj} = V_j$ to $V_{inj} = 0.5V_j$, the upper Stokes number value is increased from 4 to 19. Perhaps this is the explanation why at such high Stokes number,

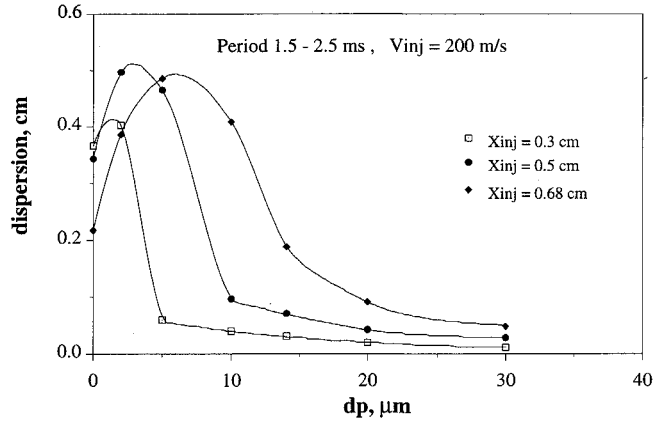

Fig. 13 Effect of injection location on dispersion; V_{inj} = 200 m/s.

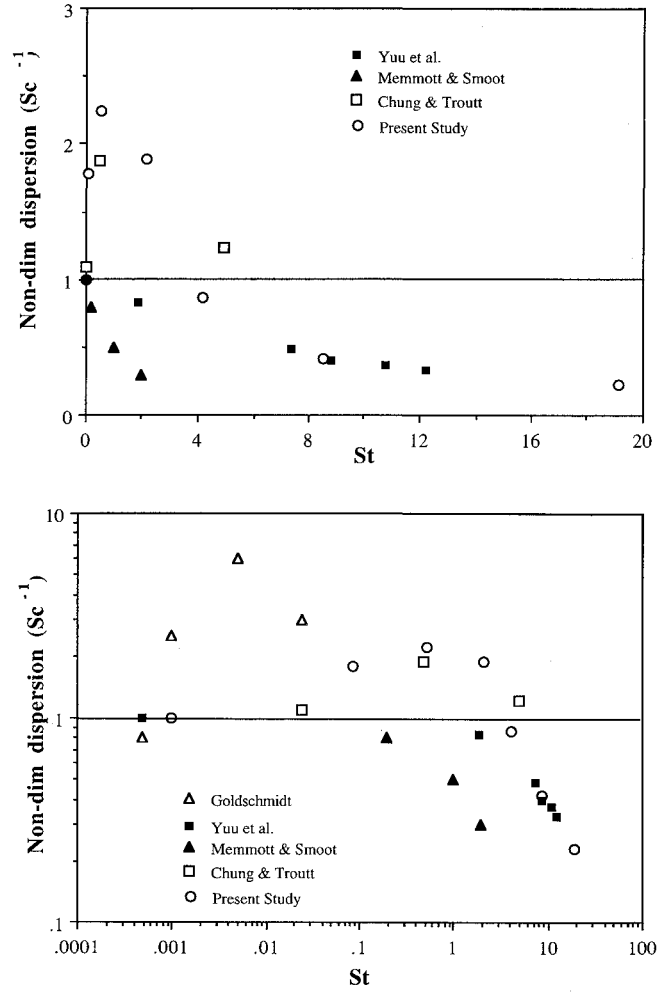

Fig. 14 Comparison with previous experimental[20,21,22] and numerical[5] results.

Longmire and Eaton[13] observe a strong convective action of ring structures on particle dispersion. Finally, the experimental study also reveals the presence of centrifugal and inertial mechanisms even though these terms are not used in defining the effect of vortex rings on particle motion. Longmire and Eaton use the term "formation of clusters" which is akin to the centrifugal mechanism defined in the present study. For Stokes number less than 11, the particle motion is governed by the centrifugal mechanism. As further stated in their paper, "for the range $11 < St < 13$, the flow structures alter the particle paths, but distinct clusters do not form," which is akin to the inertial mechanism defined in the present study.

Conclusions

Particle dispersion in a high velocity axisymmetric jet is investigated by extending the MILES approach[17] to the computation of two-phase flows dominated by large-scale vortical structures. The influence of vortex ring structures on particle dynamics in the near jet region is studied. Both the nature and dynamics of dispersion and the mechanisms responsible for it are established through detailed flow visualizations, analysis of particle motion, and quantified dispersion behavior.

Trajectories of individual particles injected from different radial locations at the nozzle exit provide a good qualitative picture of the role of large structures in the dispersion of particles. For injection locations inside the core region, only the very small particles ($St \leq 0.01$) are affected by the vortex structures. As the injection location moves closer to the shear region, the influence of ring structures on particle dynamics becomes progressively stronger. Using a detailed flow visualization, based on the streaklines for the tracer particles, and the trajectories of individual particles in a reference frame stationary with respect to ring structures, three dispersion mechanisms are identified. The very small particles, $St < 0.02$, are subjected to the vortex mechanism, whereby the particles are trapped in the vortical structures and follow the behavior of tracer particles. The centrifugal mechanism is the one most responsible for enhancing the dispersion of intermediate size particles, $0.02 < St < 4.0$. Here, the particles are confined to the periphery of the vortex structures and are flung out because of the centrifugal action as the vortex rotates. For the conditions studied, the second vortex merging has the maximum effect on particle dispersion during this particle-vortex interaction. The third mechanism, termed here as the inertial mechanism, is operative on large particles injected in the shear layer or on small particles injected in the core region. Here, the particles are not subjected to the centrifugal motion, rather their dynamics is influenced by the flow induced by vortex motion. It should be noted that the terms used to define different mechanisms are our own and not referred to as such in the literature. In this context, it is interesting to mention the particle dispersion model of Wen et al.[23] who suggest that the dispersion process involves two mechanisms operating in succession. The first one is a stretching mechanism whereby a vortex places the particles along the braid region, followed by the folding mechanism which distributes the particles along the periphery of the vortex during a pairing interaction.

Quantified dispersion analysis further establishes the existence of three dispersion mechanisms and demonstrates the size-selective nature of the dispersion process, observed previously by Chung and Troutt[5] in lower velocity jets. In addition, the quantitative results are used to identify the range of Stokes number for the three dispersion mechanisms. For the base case, the vortex mechanism is observed for $St < 0.02$, the centrifugal mechanism for $0.02 < St < 4.0$, and the inertial mechanism for $St > 4.0$. The results further indicate that the Stokes number range for the centrifugal and inertial mechanisms can be significantly modified by changing the particle injection characteristics, i.e., the injection velocity and location. For example, reducing the injection velocity from $V_{inj} = V_j$ to $V_{inj} = 0.5V_j$ significantly increases the Stokes number range for the centrifugal mechanism, from $0.02 < St < 4$ to $0.02 < St < 19$. Consequently, the Stokes number for the maximum dispersion as well as the Stokes number range for enhanced dispersion are strong functions of the particle injection location and the ratio of particle injection and jet velocity.

Results also indicate that a local flow time scale rather a global one should be used in defining the Stokes number. For the present simulations, since the second merging is seen to have the maximum effect on particle dispersion, the flow time scale is based on the second merging frequency. This definition provides a good correlation between the Stokes number and the enhanced dispersion behavior, which is further confirmed by changing the particle density. The actual numbers for the Stokes numbers just quoted will change if the characteristic flow time is defined differently. However, the emphasis of this work is on the relative values for the Stokes number and the identification and characterization of the different mechanisms responsible for particle dispersion.

The results of our numerical study are also compared with the previous numerical and experimental results. Although the comparison is found to be favorable, it also stresses the need for additional experimental studies focusing on the detailed statistical results in the near jet region. In this context, a recent experimental study due to Longmire and Eaton[13] is particularly relevant to the present work. Although a quantitative comparison with their results is not possible, many of their qualitative observations regarding the influence of vortex ring structures on particle dispersion in the near jet region are confirmed in our simulations. These include the tendency of particles to wrap around the outer edge of the structures, a wide range of Stokes number for enhanced particle dispersion at lower injection velocities, and the existence of centrifugal and inertial dispersion mechanisms at different Stokes number.

Acknowledgments

This work was supported by the Air Force Office of Scientific Research through the Wright Laboratory, Aero-Propulsion Directorate of Wright-Patterson Air Force Base. Julian M. Tishkoff is the Program Manager. The two authors at the Naval Research Laboratory were supported by the Office of Naval Research. The calculations were performed on a Cray Y-MP at NCSA (Urbana-Champaign, IL) and Pittsburgh Supercomputer Center, Pittsburgh, PA.

References

[1]Yule, A. J., "Large Scale Structure in the Mixing Layer of a Round Jet," *Journal of Fluid Mechanics*, Vol. 89, 1978, pp. 413–432.

[2]Crowe, C. T., "Review—Numerical Models for Dilute Gas Particle Flows," *Journal of Fluids Engineering*, Vol. 104, No. 3, 1982, pp. 297–303.

[3]Crowe, C. T., Gore, R., and Troutt, T. R., "Particle Dispersion by Coherent Structures in Free Shear Flows," *Particulate Science and Technology*, Vol. 3, No. 6, 1985, pp. 149–158.

[4]Chein, R., and Chung, J. N., "Effects of Vortex Pairing on Particle Dispersion in Turbulent Shear Flows," *International Journal of Multiphase Flows*, Vol. 13, No. 2, 1987, pp. 785–802.

[5]Chung, J. N., and Troutt, T. R., "Simulation Particle Dispersion in an Axisymmetric Jet," *Journal of Fluid Mechanics*, Vol. 186, 1988, pp. 199–222.

[6]Lazaro, B. J., and Lasheras, J. C., "Particle Dispersion in a Turbulent, Plane, Free Shear Layer," *Physics of Fluids A*, Vol. 1, June 1989, pp. 1035–1050.

[7]Lazaro, B. J., and Lasheras, J. C., "Particle Dispersion in the Developing Free Shear Layer, Part 1—Unforced Flow," *Journal of Fluid Mechanics*, Vol. 235, 1992, pp. 143–178.

[8]Lazaro, B. J., and Lasheras, J. C., "Particle Dispersion in the Developing Free Shear Layer, Part 2—Forced Flow," *Journal of Fluid Mechanics*, Vol. 235, 1992, pp. 179–221.

[9]Samimy, M., and Lele, S. K., "Motion of Particles with Inertia in a Compressible Free Shear Layer," *Physics of Fluids A*, Vol. 3, No. 8, 1991, pp. 1915–1923.

[10]Aggarwal, S. K., Chen, G., Yapo, J. B., Grinstein, F. F., and Kailasanath, K., "Numerical Simulation of Particle Dynamics in Planar Shear Layers," AIAA Paper 92-0107, Jan. 1992; also *Computers and Fluids* (submitted for publication).

[11]Hishida, K., Ando, A., and Maeda, M., "Experiments on Particle Dispersion in a Turbulent Mixing Layer," *International Journal of Multiphase Flows*, Vol. 18, No. 2, 1992, pp. 181–194.

[12]Grinstein, F. F., Hussain, F., and Oran, E. S., "Vortex-Ring Dynamics in a Transitional Subsonic Free Jet, A Numerical Study," *European Journal of Mechanics B/Fluids*, Vol. 9, No. 6, 1990, pp. 499–525.

[13]Longmire, E. K., and Eaton, J. K., "Structure of a Particle-Laden

Round Jet," *Journal of Fluid Mechanics*, Vol. 236, 1992, pp. 217–257.

[14]Kibens, V., "Discrete Noise Spectrum Generated by an Acoustically Excited Jet," *AIAA Journal*, Vol. 18, No. 4, 1979, pp. 434–441.

[15]Hussain, A. K. M. F., and Zaman, K. B. M. Q., "The 'Preferred Mode' of the Axisymmetric Jet," *Journal of Fluid Mechanics*, Vol. 110, 1981, pp. 39–71.

[16]Husain, Z. D., and Hussain, A. K. M. F., "Natural Instability of Free Shear Layers," *AIAA Journal*, Vol. 21, No. 11, 1983, pp. 1512–1517.

[17]Boris, J. P., Grinstein, F. F., Oran, E. S., and Kolbe, R. L., "New Insights into Large Eddy Simulation," Naval Research Laboratory, Rept. NRL/ MR/ 4400-92-6979, Washington, DC, 1992.

[18]Grinstein, F. F., Oran, E. S., and Boris, J. P., "Direct Numerical Simulation of Axisymmetric Jets," *AIAA Journal*, Vol. 25, No. 1, 1987, pp. 92–98.

[19]Ho, C. M., and Huerre, P., "Perturbed Free Shear Layers," *Annual Review of Fluid Mechanics*, Vol. 16, 1984, pp. 365–424.

[20]Yuu, S., Yasukouchi, N., Hirosawa, Y., and Jotaki, T., "Particle Turbulent Diffusion in a Dust-laden Round Jet," *AIChE Journal*, Vol. 24, No. 4, 1978, pp. 188–207.

[21]Memmot, V. J., and Smoot, L. D., "Cold Flow Mixing Rate Data for Pulverized Coal Reactors," *AIChE Journal*, Vol. 24, 1978, pp. 466–473.

[22]Goldschmidt, V., and Eskinazi, S., "Two-Phase Turbulent Flow in a Plane Jet," *Journal of Applied Mechanics*, 1966, pp. 735–747.

[23]Wen, F., Kamalu, N., Chung, J. N., Crowe, C. T., and Troutt, T. R., "Particle Dispersion by Vortex Structures in Plane Mixing Layers," *ASME Journal of Fluids Engineering*, Vol. 114, Dec. 1992, pp. 657–666.